

Suppression of General and Localized Corrosion by Air-Dried TiO₂ Nanostructured Coatings on AISI 304 Stainless Steel

A. Ivanković, S. Martinez, I. Šoić

University of Zagreb, Faculty of Chemical Engineering and Technology, Marulićev trg 19, p.p.177, HR 10000 Zagreb, Croatia

*E-mail: aivankovic8@gmail.com

Received: 21 April 2016 / *Accepted:* 20 June 2016 / *Published:* 7 August 2016

In the present study, TiO₂ dispersions were deposited on AISI 304 stainless steel and air dried. The morphology and structure of the coatings were analysed using FTIR, XRD and SEM. Open circuit potential and polarization measurements were done in the dark and under UV illumination, in 3,5% NaCl. TiO₂ nanostructured coatings on stainless steel act by forming a protective layer on the metal surface. Both, general and localized corrosion are suppressed, as the current in the passive range decreases, the corrosion and the pitting potential become more noble and the passive range broadens. The UV illumination pushes the potential of stainless steel to more negative values within the passive range, away from the pitting potential as a result of photogenerated cathodic protection current effect. The coatings have been shown to decrease the current in the passive range by up to 85% and to broaden the passive range by up to 350 mV.

Keywords: Stainless steel, Corrosion, TiO₂ coating, Photogenerated cathodic protection

1. INTRODUCTION

Corrosion resistance of stainless steel depends on a combination of alloy, surface finish and service environment [1]. Fabrication of a protective coating for stainless steel in corrosive environments is of utmost technological and economic interest. The ideal coating would: (i) provide protection against general and localized corrosion and not diminish the aesthetic appearance of stainless steel (coating transparency). From the standpoint of corrosion protection, thin nanostructured TiO₂ coatings are interesting because of their: chemical resistance, transparency, high dielectric constant and the effect photogenerated cathodic protection (CP), whereby TiO₂ coating functions as a non sacrificial anode [2-12]. Since the photogenerated CP acts only under UV illumination, the investigative efforts have been made to extend the photoresponse of TiO₂ from ultraviolet to visible

light region [9,10] to delay the potential recovery after the UV illumination is switched off (e.g. by coupling TiO₂ with SnO₂, WO₃ or MoO₃ [11]) and to obtain protective effect of the TiO₂ coating in the dark [13, 14].

Dip coating of sol gels [2-13, 15], electrophoretic deposition [12] and atomic layer deposition [14], have been investigated for applying TiO₂ coatings to stainless steels. However, these methods cannot be used under in field conditions, either due to the necessity of dipping the parts into the liquid phase [2-13], sintering at 450–550 °C [2-11, 13], or applying the sophisticated equipment [14]. This study focuses on suitability of aqueous dispersions of TiO₂ nanoparticles to be applied by the technique of high volume low pressure (HVLP) air spraying, or in a form of a drop and air dried, for the protection of AISI 304 stainless steel against general and localized corrosion.

Controlling the dispersion and aggregation of the nanoparticles is crucial to exploiting the advantages of their nanometric size. For that purpose, apart from the pristine TiO₂ nanoparticle dispersions in doubly distilled water, formulations in HNO₃ of pH = 2, and those containing the addition of NaNO₃ and a commercial dispersant, have been investigated. The coatings structure and protective efficacy were investigated by various electrochemical (open circuit potential measurements, polarization measurements) and non electrochemical techniques (SEM, EDX, FTIR, XRD). The protective action of the coatings, both in the dark and under UV illumination, is explained in terms of the electronic properties of stainless steel, TiO₂ and the solution.

2. EXPERIMENTAL DETAILS

For the preparation of TiO₂ nanoparticle aqueous dispersions, PC10, anatase phase particles (in further text denoted by NP TiO₂) with a declared average diameter of 10 nm manufactured by TiPE, Shanghai, have been used.

Altogether, four coating formulations have been tested.

The first two formulation were prepared in a way that 0.1 g of TiO₂ nanoparticles was dispersed in 100 ml of double distilled water, in the first case, and the solution of nitric acid of pH = 2, in the second case. Additionally, another two formulations were prepared by supplementing pH = 2 dispersion with additives. One of the additives was, Disperbyk 2012 produced by Byk, and the other one was NaNO₃. The concentration of additives was 10 wt % with respect to the mass of TiO₂. After adding all the components to the doubly distilled water, the mixtures were subjected to ultrasonic agitation for 15 minutes using an ultrasonic mixing device Bandelin Sonopuls HD 2200 and the probe KE 76 made of titanium alloy. The probe operated at 20 kHz and at 72% of its nominal power of 200 W. For comparison, the experiments were also done on bare stainless steel electrode and with the nitric acid of pH = 2, without TiO₂ particle addition. X-ray diffraction (XRD) analysis has been performed on nanoparticles powder using Philips PW 1830 HT generator, Ni filtered CuK α radiation tube, PW 1050 vertical goniometer with step scanning motor, proportional counter, PW3710 control electronics and system software. Analysis is made using characteristic radiation of copper cathodes to scan the samples between 5° and 80°, K α lines.

Fourier transform infrared (FTIR) spectra were recorded using a PerkinElmer spectrometer Spectrum One, USA. Spectra were obtained in the range from 400 to 4000 cm^{-1} , each spectrum being an average of ten scans with a resolution of 4 cm^{-1} . For the first sample, 3 mg of nanoparticle powder was mixed into 350 mg of spectroscopically pure KBr while for the second sample, 350 mg of KBr was rubbed into the surface of the steel electrode covered by spray applied and dried coating. Samples bearing KBr was then hydraulically pressed into a 13 mm stainless steel die and the two resulting pellets further subjected to FTIR measurement. Preparation of pellets conformed with the standard ASTM E1252:2007 [16].

SEM and EDX analysis was recorded using Tescan Vega III, SBU EasyProbe scanning electron microscope with 10 kV accelerating voltage of the electron beam at various magnifications.

For the electrochemical tests, AISI 304 specimen were abraded with wet 600, 800 and 1200 grit SiC paper, degreased with ethanol in an ultrasonic bath for 5 minutes, and then air dried. Electrolyte exposed metal area was a circle 1 cm in diameter. Coating was sprayed onto the electrode surface by high volume low pressure (HVLP) method using pressure of 2.5 bar or applied as a 300 μl drop. In the first case, 24 h long air drying was done in vertical position, and in the second in horizontal position. Spraying method was also used by Momeni et al. in the case of sol-gel coatings [17].

Polarization tests were performed in 3.5% NaCl solution prepared with analytical grade NaCl and deionised water. The stainless steel AISI 304 with an active area of 1 cm^2 were used as the working electrode, a SCE as the reference electrode and a graphite rod served as a counter electrode, respectively. Electrochemical test were done on Palm Sens 3, Potentiostat/Galvanostat/Impedance Analyzer. The scan rate in all the experiments was 1 mV s^{-1} . The measurement regime conformed with the procedure for testing passive metallic materials described in standard ISO 17475:2005 [18].

The lamp used to introduce UV irradiation was Blacklight 368, produced by Sylvania, emitting UV light of 368 nm. The lamp was inserted into the quartz glass tube that was inserted into the cell. Open circuit potential (OCP), UV on/off potential measurements were started immediately after electrode immersion and the OCP was recorded every second, for 600 s. On and off periods exchanged every 100 s or 1000 s starting with UV off state.

In separate experiments, potentiodynamic polarization scan was initiated after 1 h of specimen stabilization in the solution. The value of potential attained after stabilization was recorded and termed as the corrosion potential (E_{corr}). The scan was started from E_{corr} and stopped when the current reached 10^{-4} A. Each polarization experiment was done in the dark and under UV light. In experiments with UV lamp the temperature of the solution increased due to the lamp presence, and stabilized at 40 ± 0.5 °C after 15 minutes, well before the commencement of polarization.

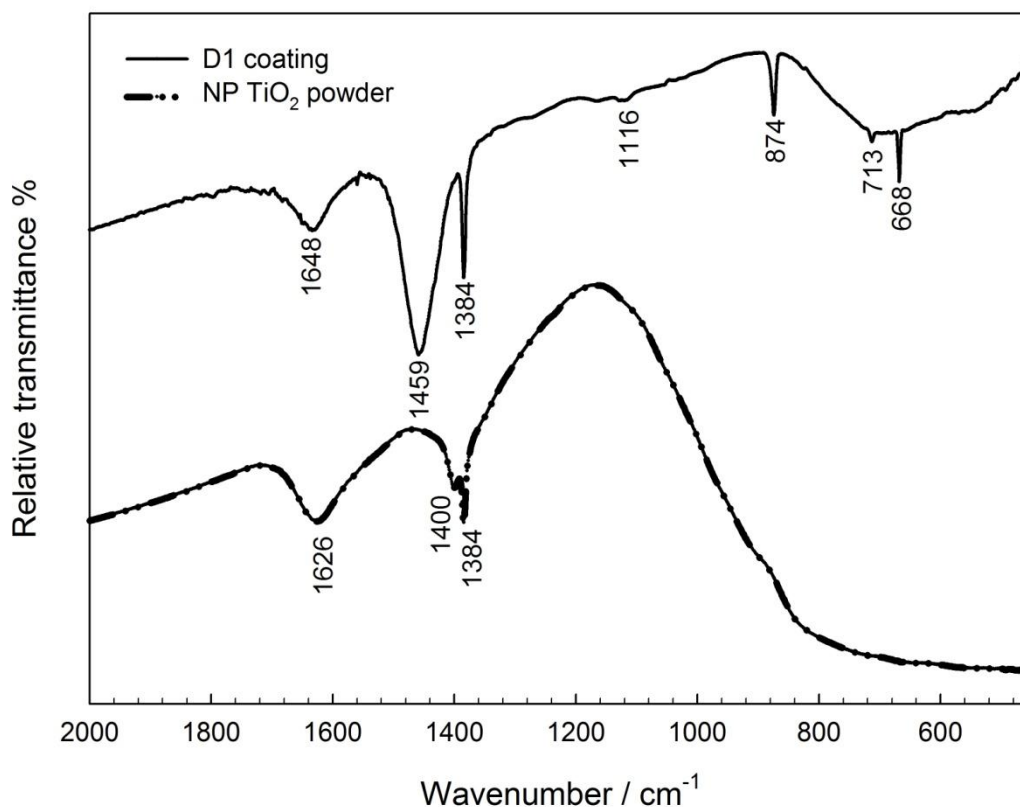
In the tables, as well as in the figures throughout the text, various formulations applied by different methods, are denoted by abbreviations that relate to their composition and technique of application. These abbreviations are given in the following table:

Table 1. Various formulations of TiO₂ coating denoted by abbreviations that relate to their composition.

SYSTEM	ABBREVIATION
AISI 304	NO
HNO ₃ pH=2 - drop applied	D0
HNO ₃ pH=2 - spray applied	S0
TiO ₂ - drop applied	D1
TiO ₂ - spray applied	S1
TiO ₂ + HNO ₃ pH=2 - drop applied	D2
TiO ₂ + HNO ₃ pH=2 - spray applied	S2
TiO ₂ + HNO ₃ pH=2 + NaNO ₃ - drop applied	D3
TiO ₂ + HNO ₃ pH=2 + Disperbyk - drop applied	D4

3. RESULTS AND DISCUSSION

3.1. FTIR

**Figure 1.** FTIR spectra of KBr pastilles with the TiO₂ nanoparticles powder (NP TiO₂) and the nanoparticle coating D1 scratched from surface of AISI 304 stainless steel.

The spectrum of TiO₂ nanopowder and of the surface acquired sample in the case of the coating denoted by D1, are shown in Fig. 1. The spectrum of TiO₂ nanopowder shows characteristic vibrations of the inorganic Ti–O stretch as a broad band in the range 450–800 cm⁻¹ [15]. The sharp band in both samples at 1385 cm⁻¹ may be attributed to the NO₃⁻ groups from the peptization process because of the addition of HNO₃ [19]. Spectrum of the sample D1 acquired from the electrode surface also shows the broad Ti–O band but with superimposed smaller sharp absorption bands at 874, 713, and 668 cm⁻¹. CO₂ capture and the formation of carbonate and bicarbonate species has previously been confirmed spectroscopically on surface of hydrated TiO₂ anatase [20, 21]. Hence, bands at 874 and 713 are probably due to $\nu_2(\text{CO}_3^{2-})$ in plane bend and $\nu_4(\text{CO}_3^{2-})$ out of plane bend.

The bands at 1400 and 1459 cm⁻¹ may be attributed to $\nu_{as}(\text{CO})$ and the band at 1116 cm⁻¹ to $\nu_{ss}(\text{CO})$ of the bicarbonate ions [21]. The band at 668 cm⁻¹ represents angle bending $\nu_B(\text{COC})$. Bands at 1626 and 1648 cm⁻¹ are due to the influence of water. The difference in wavenumbers of the asymmetric and the symmetric bands indicates formation of bidentated bicarbonates whereby the –HCO₃ interacts through two oxygens with two adjacent Ti sites leading to the formation of an O–C–O bridging structure [20, 22]. This is particularly visible for the surface acquired sample which has less intense Ti–O band that does not completely overlap the characteristic bicarbonate bands.

3.2. XRD

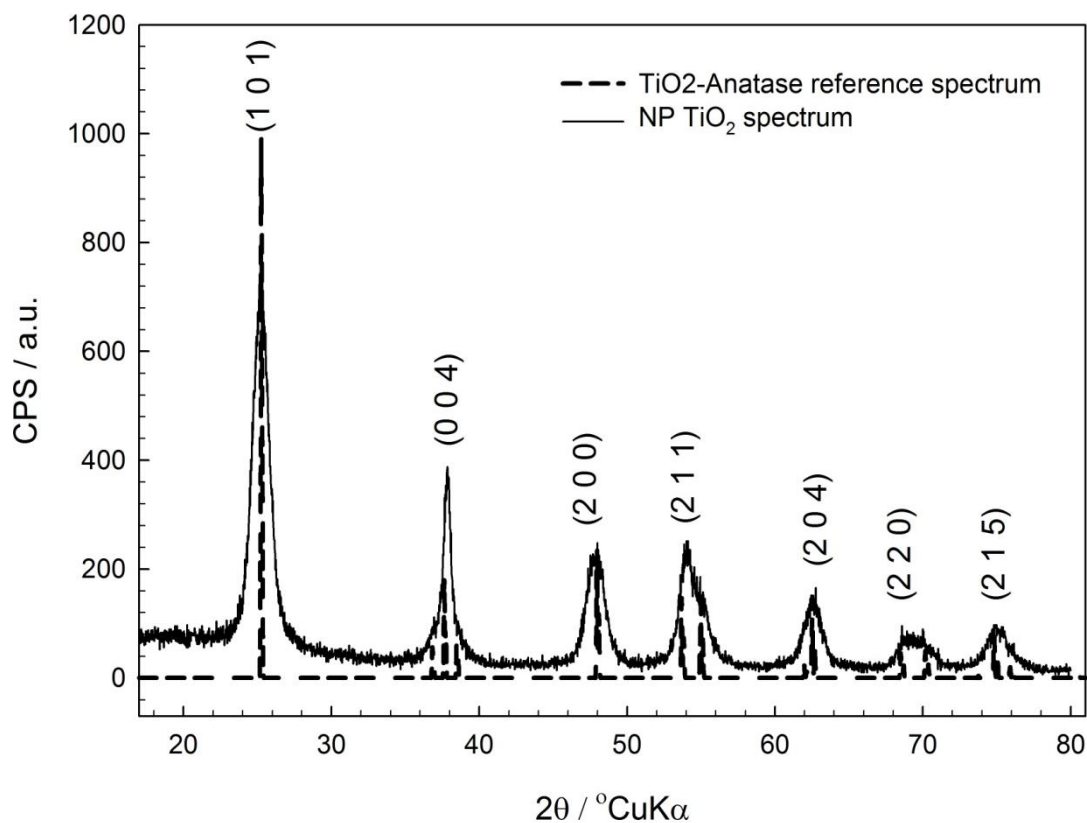


Figure 2. XRD of TiO₂ anatase reference spectrum and bare TiO₂ nanoparticles used in this study.

The XRD patterns in Fig. 2 show peaks at 2θ values of 25.3, 37.8, 48.2, 54.0, 62.5, 68.5, and 74.8° attributed to reflections of the crystal planes (1 0 1), (0 0 4), (2 0 0), (2 1 1), (2 0 4), (2 2 0), and (2 1 5) of anatase [4]. No other crystalline phase was observed. The average crystallite size, calculated using Scherrer equation from the (1 0 1) reflection of anatase is 5.67 nm. The nominal radius of nanoparticles of 10 nm is larger than the calculated crystallite size suggesting their multi crystallite structure [6]. Crystalline phase was assigned to anatase ICDD PDF#21-1272 [23]. The observed high crystallinity, anatase phase material, small crystallite size and small particle size declared by the particle producer, should ensure photoactivity of TiO₂ nanoparticles used in this study [24]. Despite some degree of agglomeration that would happen during coating production and application, the particles of the observed quality should, according to the observations from the literature [25, 26], still provide sufficient exposed titania sites on which photocatalytic reaction can takes place.

3.3. SEM/EDX of the coating

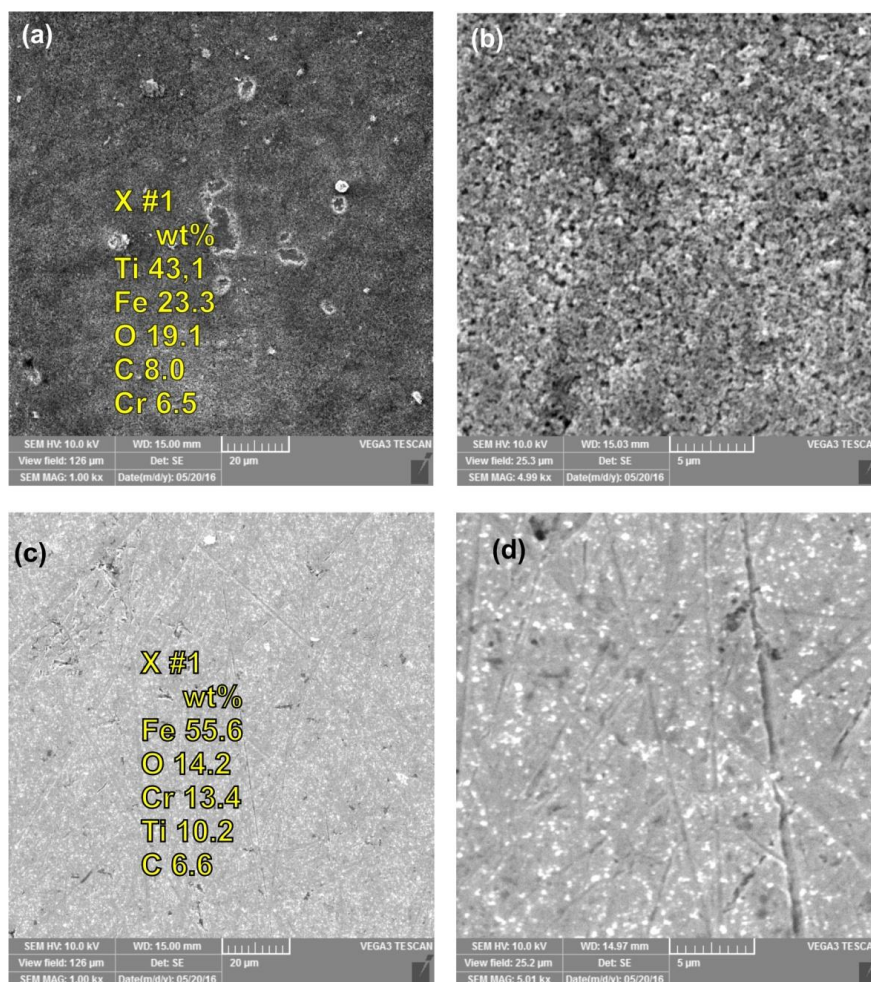


Figure 3. SEM micrographs at various magnifications and EDX results for the drop applied coating D1 (a) enlarged 1000 × and (b) enlarged 5000 × and the spray applied coating S1, (c) enlarged

1000 × and (d) enlarged 5000 ×, at the surface of AISI 304 stainless steel.

Typical appearance of all the spray and the drop applied TiO₂ layers is shown in the SEM micrographs in Fig. 3. D1 and S1 coatings were chosen to exemplify the appearance. Aggregates of the nanoparticles are observed at the surface of the both layers. The original topography of the substrate (polishing marks), visible below the TiO₂ coating, is pronounced for the spray applied sample. At the highest magnification, it can be noted that the drop applied coating film is composed of densely packed random agglomeration of TiO₂ nanoparticles. The overall appearance of the surface of the coating is rough and bulgy. The appearance of the coatings is similar to the observations of other authors [5, 6, 10, 11].

EDX data, in Figs. 3 a) and c), show approximately 10% of Ti element at the surface for the sprayed coatings and 40% for the drop applied coatings. The corresponding EDX spectra are shown in Figs. 4 a) and b), respectively. However, these results should be taken with caution since the X-rays of EDX penetrate the volume of material about 1 – 2 μm in depth, and therefore for the investigated systems, probably reflect the composition of the base material to a great extent.

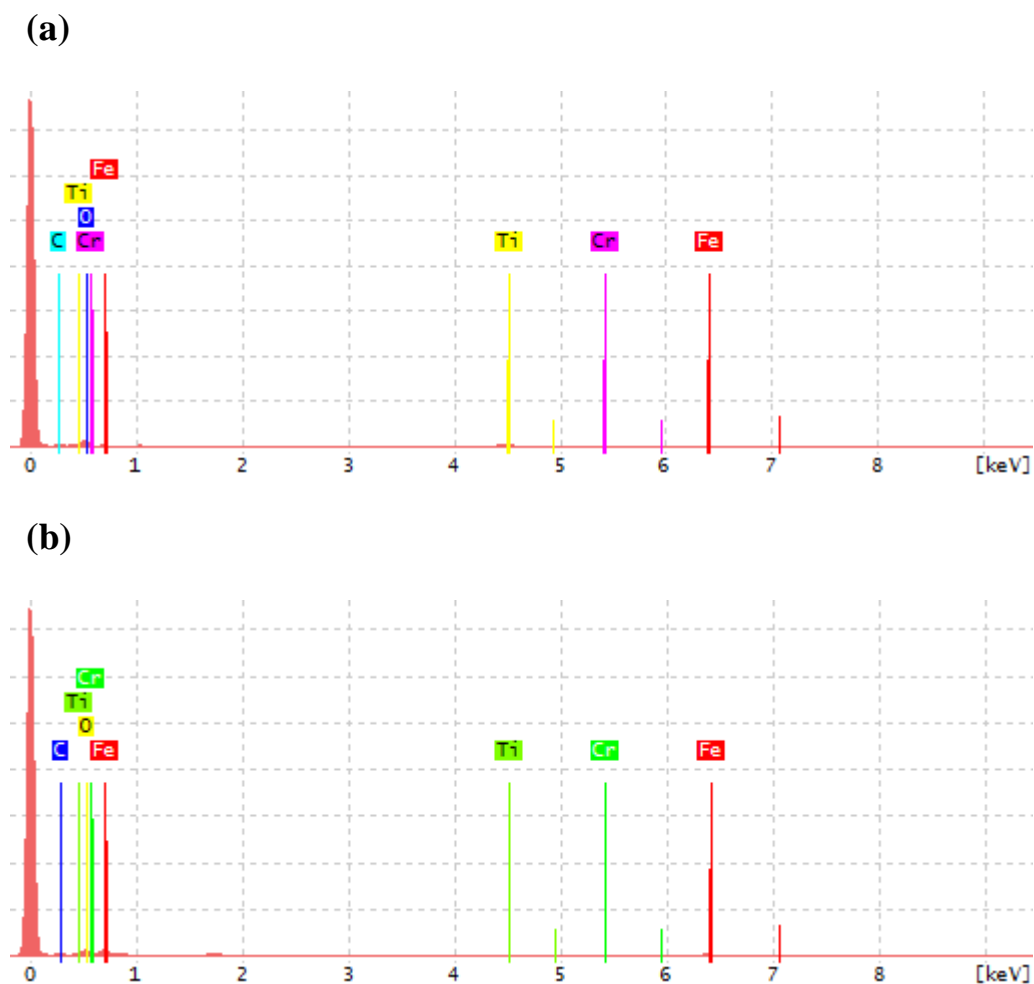


Figure 4. EDX spectra of nanostructured TiO₂ coating, for the drop applied coating D1 #1, (a), and the spray applied coating S1 #1, (b) at the surface of AISI 304 stainless steel.

3.4. Open Circuit Potential

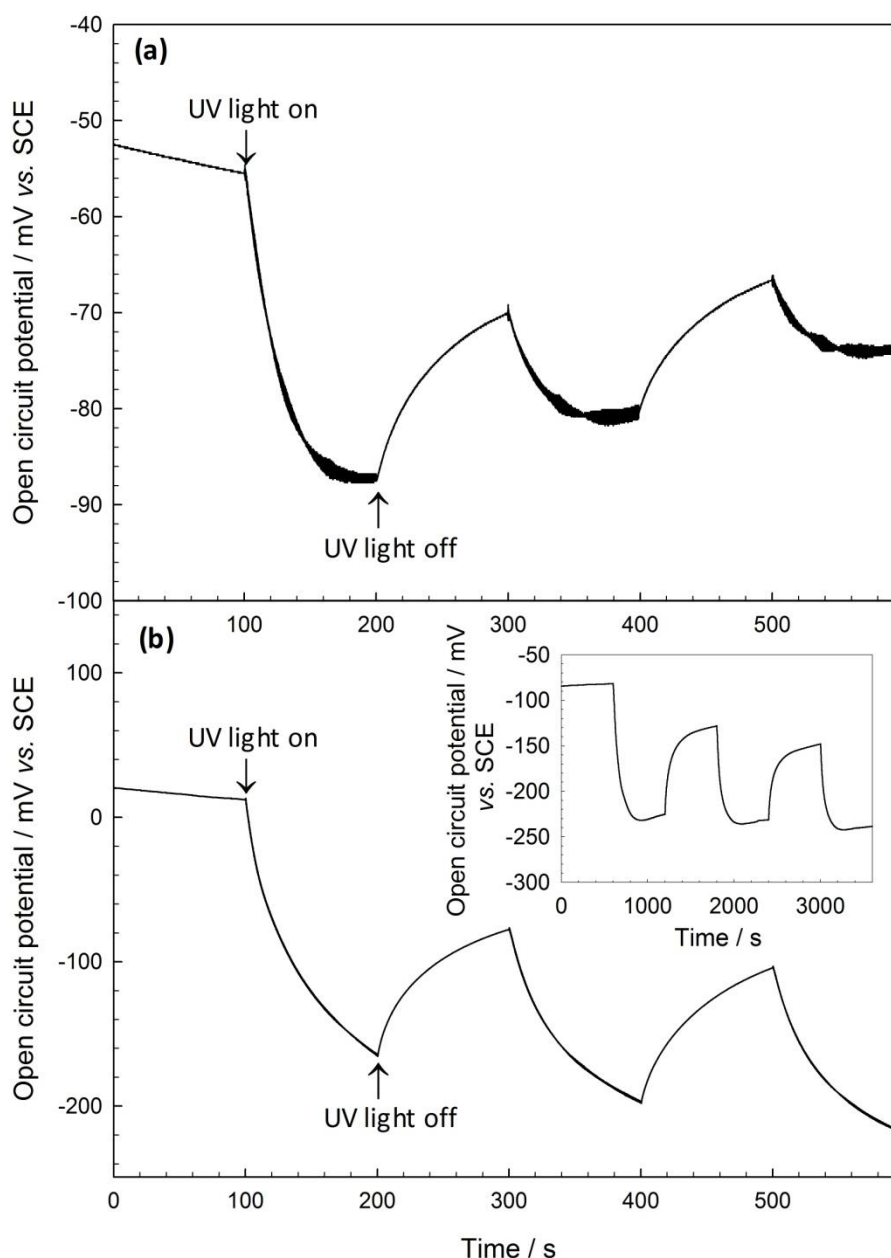


Figure 5. The open circuit potential changes of AISI 304 stainless steel covered with: (a) the spray S1 and (b) the drop-applied D1 TiO₂ layers under UV on/off conditions in 3,5% NaCl solution.

It is well known that TiO₂ (anatase) is a n-type semiconductor with the band width of 3.2 eV [14]. The photoactivity of sol-gel TiO₂ anatase nanoparticle coatings has been well documented [9-14]. In the case of the coating consisting of small TiO₂ nanoparticles, the band structure in the TiO₂ is interconnected through the TiO₂ grain boundaries forming continuous conduction band electron transporting channels from the semiconductor/electrolyte to reach semiconductor/substrate interface [27]. When the UV illumination is switched on, accumulation of photogenerated electrons in TiO₂

causes the shift of its quasi Fermi level to higher energies. Electrons moves towards the stainless steel substrate and holes towards the TiO₂ surface, therefore polarizing the stainless steel negatively. When the UV illumination is switched off, the present electrons and holes recombine and OCP suddenly increases.

Typical charge and self discharge of stainless steel covered with the spray and the drop applied TiO₂ layers under UV on/off conditions is presented in Fig. 5 a) and b) is similar to the observations of other authors [7-9, 11, 14]. D1 and S1 coatings were chosen to exemplify typical UV on/off behaviour. The OCP measurements were done immediately after immersion of the electrode into the solution. The initial OCP of the D1 coating equals +20 mV_{SCE} and is higher by 72 mV than the OCP of the S1 coating, which equals -52 mV. The negative potential shift after 100 s of UV irradiation equals -35 mV for the S1 coating and -190 mV for the D1 coating. The inset of Fig. 5 b) shows continuation of measurement for the D1 coating, but with longer (1000 s) UV on/off intervals. It may be concluded that the drop applied film is thicker, and hence gives more pronounced negative potential shift but also exerts longer potential stabilisation time.

3.5. Anodic potentiodynamic polarization

To mimic the in service conditions of the coating (exposure in humid atmosphere with high chloride contamination during day and night), the experiments in the dark were done at the room temperature (23±0.5 °C), while those under UV irradiation were done at the temperature of 40±0.5 °C.

Polarization was performed after the stable potential values were reached, after 1 h of stabilization in the solution. These values of potential were termed E_{corr} and are given in Tables 2 and 3.

Application of pure HNO₃ solution of pH = 2 to the stainless steel surface yields increased E_{corr} with respect to the bare electrode. This result is in concordance with the fact that HNO₃ is a known stainless steel passivator and also purports the idea that the increase in the E_{corr} may be interpreted by the enhancement of the passive layer due the action of highly oxidizing species.

Similarly, measured in the dark, the E_{corr} of coated stainless steel, is in all cases, more noble than the E_{corr} of bare stainless steel. Generally, higher E_{corr} measured in the dark for TiO₂ coated stainless steel, is interpreted as an indicator of the protective barrier nature of the coating [6, 11, 13, 28].

The anodic potentiodynamic polarization curves of stainless steel, without or with the coatings under light off and light on conditions are shown in Fig. 6. Tables 2 and 3 list: (i) the pitting potential, E_p , (ii) the width of the passive range i.e. the difference between the pitting and the corrosion potential, $E_p - E_{\text{corr}}$ and (iii) the passive current, I_p . I_p was extracted from the anodic polarization curve at an anodic polarization of +200 mV from E_{corr} . For all systems, the potentials at which I_p was determined, were located almost the middle of the passive range. Current in the mid passive region is considered representative of the passive state [29, 30].

The percentual decrease of the passive current I_p by obtained on coated v.s. uncoated samples has been termed the coating efficiency and has been calculated according to the following equation:

$$\text{Coating efficiency} = \frac{I_{p(\text{no coating})} - I_{p(\text{coating})}}{I_{p(\text{no coating})}} * 100\% \tag{1}$$

The coating efficiency is shown in the last column of Tables 2 and 3.

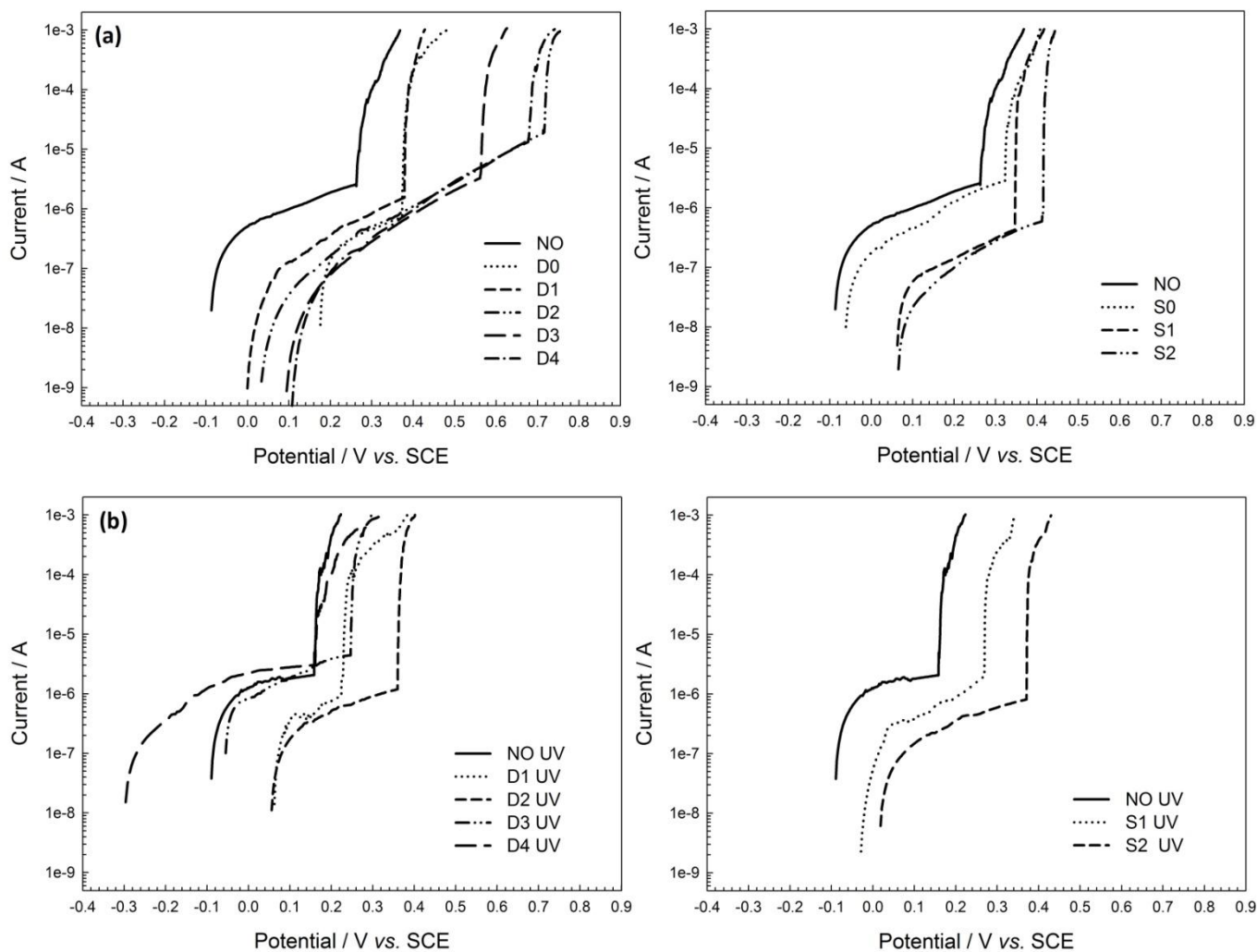


Figure 6. Polarization curves for bare and TiO₂ coated AISI 304 stainless steel specimens in 3,5% NaCl for: the drop applied systems, (a) without and (b) with UV irradiation, and for the spray applied systems, (c) without and (d) with UV irradiation.

First, the uncoated and coated specimens may be compared..

Both, in the dark and under UV irradiation, TiO₂ coated specimens have lower I_p with respect to the uncoated specimens, therefore the efficiencies of the coatings are > 0 (except for the illuminated D3 coating).

It is further interesting to compare illuminated and unilluminated systems.

For bare stainless steel, approximately two fold increase in I_p and a -100 mV shift of the pitting potential is observed under UV light irradiation with respect to UV non-illuminated systems. Hence,

bare stainless steel is more susceptible to uniform and pitting corrosion, probably due to the temperature effect.

For the coated systems, higher I_p and lower coating efficiency are observed under UV light irradiation with respect to UV non-illuminated systems. Hence, coated stainless steel is also more susceptible to uniform and pitting corrosion. As previously observed on sol-gel TiO₂ nanoparticle coatings [11], it is probable that the coated systems exert the influence of photocurrent together with the influence of temperature increase, therefore yielding lower efficiency.

Table 2. Electrochemical parameters: corrosion potential, E_{corr} , pitting potential E_p , width of the passive range, $E_p - E_{\text{corr}}$, current in the passive range I_p , and coating efficiency, for nanostructured TiO₂ coatings on AISI 304 stainless steel electrode in 3,5 % NaCl solution in the dark.

SYSTEM	$E_{\text{corr}}/$ mV	$E_p/$ mV	$E_p - E_{\text{corr}}/$ mV	$I_p/$ μA	Coating efficiency / %
NO	-86	257	343	0.814	-
D0	176	374	198	0.541	33.5
S0	-61	323	384	0.426	47.7
D1	0	371	371	0.206	74.7
S1	63	344	281	0.155	81.0
D2	34	718	684	0.134	83.5
S2	66	412	346	0.123	84.9
D3	95	556	462	0.149	81.7
D4	107	677	570	0.196	75.9

Table 3. Electrochemical parameters: corrosion potential, E_{corr} , pitting potential E_p , width of the passive range, $E_p - E_{\text{corr}}$, current in the passive range I_p , and coating efficiency, for nanostructured TiO₂ coatings on AISI 304 stainless steel electrode in 3,5 % NaCl solution, under UV irradiation.

SYSTEM	$E_{\text{corr}}/$ mV	$E_p/$ mV	$E_p - E_{\text{corr}}/$ mV	$I_p/$ μA	Coating efficiency/ %
NO UV	-90	157	247	1.784	-
D1 UV	63	224	161	0.841	52.9
S1 UV	-29	270	299	0.433	75.7
D2 UV	53	360	307	0.537	69.9
S2 UV	19	371	390	0.262	85.3
D3 UV	-55	246	301	1.799	-0.8
D4 UV	-296	161	457	0.791	55.7

Pitting corrosion susceptibility decreases as the breakdown potential shifts noble and departs from the open circuit potential [18]. A noble shift in the E_p is observed for all the investigated coatings. Also, the increase in the $E_p - E_{\text{corr}}$ difference is observed for almost all the coated samples and is

particularly pronounced the drop applied coatings prepared at pH = 2, D2, D3 and D4. Comparison to the results with only HNO₃ of pH = 2 applied to the surface, indicates that the protective effect is due to TiO₂ nanoparticle presence, and not to HNO₃.

Altogether, D2 formulation gives the best result when both the efficiency of suppressing general and localized corrosion are considered.

3.6. SEM micrographs of the pitting morphology

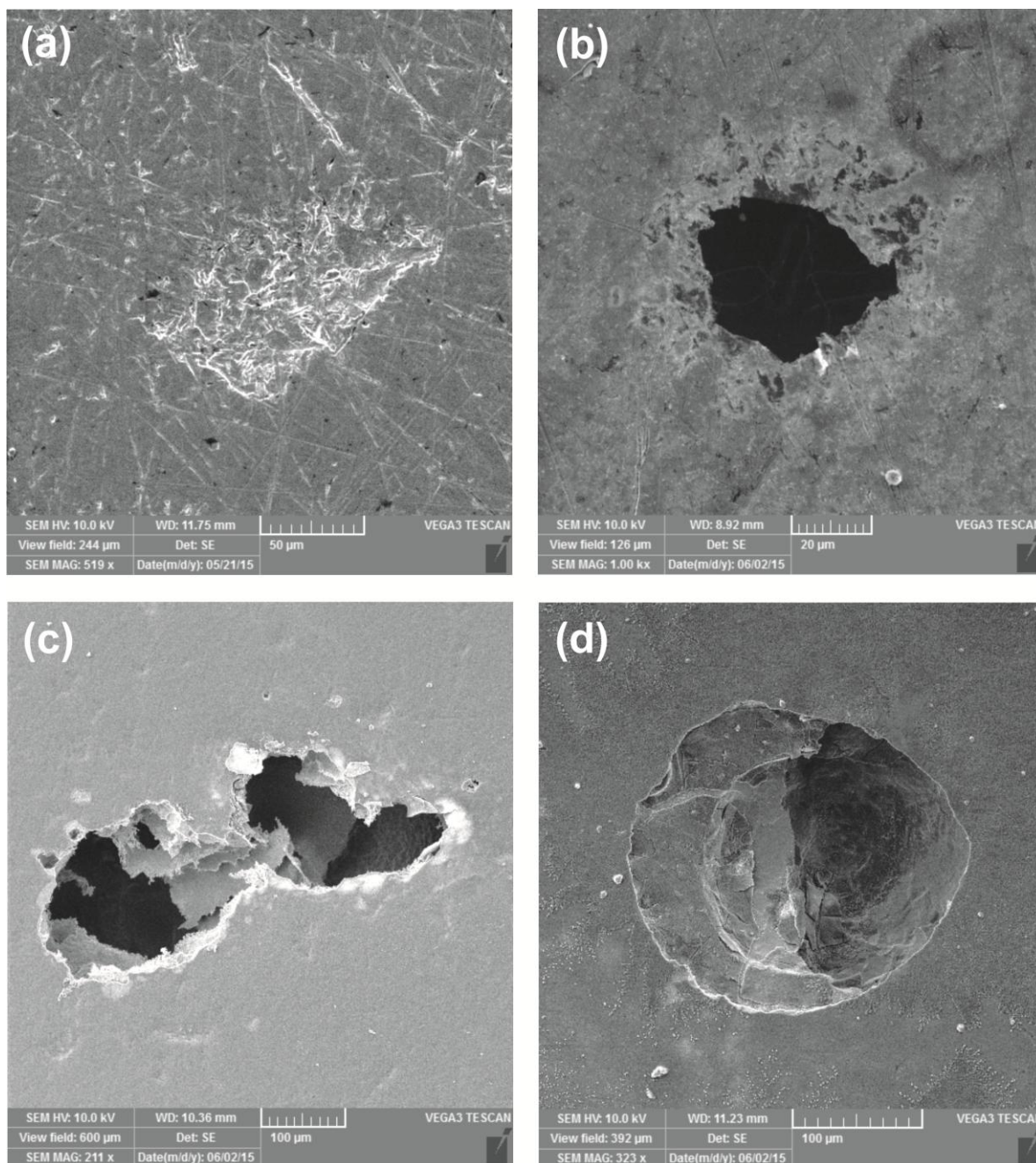


Figure 7. SEM micrographs of pits on the surface of AISI 304 stainless steel after pitting potential measurements in 3.5% NaCl solution for systems: (a) NO magnified 500 × and (b) S2 magnified

1000 ×, (c) D3 magnified 200 × and (d) D4 magnified 300 ×.

After the polarization experiments, the corrosion damage at the bare stainless steel surface (system N0) consists of the shallow recesses showing morphology of intergranular attack, as seen in Fig. 7 a). Also on bare stainless steel surface and on surface with spray applied coatings, small pits, approximately 25-50 μm in diameter, are seen. A pit obtained for system S2 was chosen as an example and shown in Fig. 7 b). Drop applied coatings show highly localized, deep pitting, as seen from Figs. 7 c) and d). Here, systems D3 and D4 were taken as examples in Figs. 7 c) and d), respectively. No intergranular attack is seen at the coated samples

The observed pit morphology, together with the decrease in I_p and increase in E_p , indicate protective action of TiO₂ coatings. The pits formed at the coated surfaces are larger and their shape and depth are representative of a stable pit form. It is known that the geometry of the pit is dependent on the polarization potential and the local pit current density at which the pit grows [31, 32]. As the potential at which the pit grows becomes more anodic and the current density higher pit becomes larger and the pit mouth become more open and of less regular shape. It may be concluded that, on coated surfaces, the pits have propagated at a higher potentials and pit current densities, therefore allowing for a broader passive region.

4. CONCLUSION

The investigated nanostructured coatings of TiO₂ exert protective action on AISI 304 stainless steel that may be observed as a decrease of the current in the passive range, the ennoblement of the pitting potential and the broadening of the passive range. Under UV illumination, the open circuit potential shifts to more negative values as a consequence of the photogenerated cathodic protection effect. It has been shown that a protective nanostructured TiO₂ coating may be obtained on stainless steel by simple HVLP method which provides an opportunity for development of water based coating formulations suitable for use in field.

ACKNOWLEDGEMENT

We acknowledge the financial support from the University of Zagreb, Croatia through short term financial support for research in 2014, TP1.39: The development of an aqueous dispersion of TiO₂ nanoparticles with applications in the protection of metal surfaces from corrosion.

References

1. P. Rostron, C. Belbarak, *Mater. Performance*, 54 (2015) 1.
2. B. Burnat, J. Robak, D. Batory, A. Leniart, I. Piwoński, S. Skrzypek, M. Brycht, *Surf. Coat. Technol.*, 280 (2015) 291.
3. B. Burnat, G. Dercz, T. Blaszczyk, *J. Mater. Sci. - Mater. Med.*, 25 (3) (2014) 623.
4. G.X. Shen, Y.C. Chen, C.J. Lin, *Thin Solid Films*, 489 (2005) 130.

5. G.X. Shen, Y.C. Chen, L. Lin, C.J. Lin, D. Scantlebury, *Electrochimic Acta*, 50 (2005) 5083.
6. H. Yun, J. Li, H.B. Chen, C.J. Lin, *Electrochim. Acta*, 52 (2007) 6679.
7. X. Guo, W. Liu, L. Cao, G. Su, H. Xu, B. Liu, *Appl. Surf. Sci.*, 283 (2013) 498.
8. W. Liu, Y.G. Wang, G. Su, L.X. Cao, M.L. Sun, X.Q. Guo, H.M. Xu, R.J. Duan, *Carbon* 50, (2012) 3641.
9. M. Sun, Z. Chen, J. Yu, *Electrochim. Acta*, 109 (2013) 13.
10. H. Wang, Z. Wang, H. Hong, Y. Yin, *Mater. Chem. Phys.*, 124 (2010) 791.
11. M. Zhou, Z. Zeng, L. Zhong, *Corros. Sci.*, 51 (2009) 1386.
12. J.H. Park, J.S. Kim, J.M. Park, *Surf. Coat. Technol.*, 236 (2013) 172.
13. A. Balamurugan, S. Kannan, S. Rajeswari, *Mater. Lett.*, 59 (2005) 3138.
14. L. Straka, Y. Yagodzinsky, H. Kawakami, J. Romu, R. Ilola, H. Hämmnen, *Thin Solid Films*, 517 (2008) 641.
15. T. Ivanova, A. Harizanova, M. Surtchev, *Mater. Lett.*, 55 (2002) 327.
16. ASTM Standard E1252, 2007, General Techniques for Obtaining Infrared Spectra for Qualitative Analysis, *ASTM International*, West Conshohocken, PA, 2007, DOI: 10.1520/E1252-98.
17. M. Momeni, F. Golestani-Fard, H. Saghafian, N. Barati, A. Khanahmadi, *Appl. Surf. Sci.*, 357 (2015) 1902.
18. Technical Committee ISO/TC 156, ISO 17475, *Corrosion of metals and alloys*, Corrosion of metals and alloys - Electrochemical test methods - Guidelines for conducting potentiostatic and potentiodynamic polarization measurements, 2005.
19. L. Tongxu, L. Fangbai, L. Xiangzhong, *J. Hazard. Mater.*, 152 (2008) 347.
20. K. Manveen, N.K. Verma, *J. Mater. Sci. Technol.*, 30 (2014) 328.
21. L. Mino, G. Spoto, A. M. Ferrari, *J. Phys. Chem.*, C 118 (2014) 25016.
22. L.F. Liao, C.F. Lien, D.L. Shieh, M.T. Chen, J.L. Lin, *J. Phys. Chem.*, B 106 (2002) 11240.
23. ICDD Database: <http://www.icdd.com/>
24. B.S. Shirke, P.V. Korake, P.P. Hankare, S.R. Bamane, K.M. Garadkar, *J Mater Sci: Mater Electron.*, 22 (2011) 821.
25. F.A. Deorsola, E.D. Vallauri, *J. Mater. Sci.*, 43 (2008) 3274.
26. X. Jia, W. He, X. Zhang, H. Zhao, Z. Li, Y. Feng, *Nanotechnology* 18, (2007) 075602.
27. R. Beranek, *Adv. Phys. Chem.*, 786759 (2011) 20.
28. C.X. Shan, X. Hou, K.L. Choy, *Surf. Coat. Technol.*, 202 (2008) 2399.
29. B. Basu, S.Nath, *Materials for orthoedic appllications.*, In: B .Basu, D.S. Katti, A .Kumar, eds. *Advanced Biomaterials: Fundamentals, Processing, and Applications*. Hoboken, NJ: John Wiley & Sons Inc., (2009) pp 82.
30. A. Robina, G. Silvab, J.L. Rosaa, *Materials Research.*, (2013) 16(6) 1254.
31. P.C. Pistorius, G.T. Burstein, *Corrosion Science.*, 33 12 pp. (1992) 1885.
32. W.M. Tian, Y.J. Ai, S.M. Li, N. Du, C. Ye, *Technique. Acta Metallurgica Sinica(English Letters)*, 28(4) 430.